Remote Sensing of Environment 278 (2022) 113073

Contents lists available at ScienceDirect

Remote Sensing of Environment

journal homepage: www.elsevier.com/locate/rse

Near-real-time monitoring of land disturbance with harmonized Landsats 7–8 and Sentinel-2 data

Rong Shang [a,*], Zhe Zhu [a], Junxue Zhang [a], Shi Qiu [a], Zhiqiang Yang [b], Tian Li [a], Xiucheng Yang [a]

[a] *Department of Natural Resources and the Environment, University of Connecticut, Storrs, CT 06269, United States*
[b] *USDA Forest Service, Rocky Mountain Research Station, Ogden, UT 84401, United States*

A R T I C L E I N F O

Edited by Marie Weiss

Keywords:
Near-real-time
Land disturbance
Forgetting Factor
Time series analysis
NRT-MONITOR
Change detection

A B S T R A C T

Land disturbance can increase carbon emissions, cause detrimental environmental impacts, and threaten human life and property. Monitoring land disturbance in near-real-time is essential to mitigate their negative effects and prevent future losses. However, rapid and timely monitoring of land disturbance at a high spatial resolution is in its infancy. Here, we developed an algorithm for Near-Real-Time MOnitoring of laNd dIsturbance based on Time-series of harmOnized Reflectance (NRT-MONITOR) from Landsats 7–8 and Sentinel-2 data at 30-m spatial resolution. It incorporates an online recursive algorithm called Forgetting Factor to improve efficiency in the determination of land disturbance to get fast detection based on the harmonized data. This algorithm is developed and validated by using 1200 samples created from the harmonized Landsats 7–8 and Sentinel-2 time series from 2015 to 2019 within the conterminous United States (CONUS). An overall accuracy of 70% has been achieved for monitoring a variety of land disturbance types. NRT-MONITOR improves the processing efficiency (11.5 times faster) compared to the COLD algorithm (Zhu et al., 2020). The mean time lag of NRT-MONITOR, defined as the delta days of confirming a land disturbance after its occurrence, is only 35 days, which is achieved by using the harmonized Landsats 7–8 and Sentinel-2 observations and reduced number of clear observations (from six to four) needed to confirm a land disturbance. Finally, NRT-MONITOR can be integrated into an alerting system to provide potential land disturbance probability maps that are updated every three days.

1. Introduction

Land disturbance, defined as any discrete event that occurs outside the range of natural variability of the land surface (Zhu et al., 2020), are changing our planet at an alarming rate by a variety of causes, such as more frequent wildfires (Kato et al., 2020; Westerling et al., 2006), severe hurricanes (Emanuel, 2005), widely spread insect infestation (Senf et al., 2017), extensive deforestation (Potapov et al., 2019), and a rapid increase of urbanization (Ma et al., 2015). These land disturbances can increase carbon emissions, cause detrimental environmental impacts and biodiversity losses, and threaten human life, property, and local economy (Tang et al., 2019; Verbesselt et al., 2012; Zhu et al., 2020). Knowing where the land disturbance is occurring in Near-Real-Time (NRT) is essential for mitigating their negative effects and preventing future losses.

Optical satellite remote sensing continuously observes land surfaces over a large area, and the availability of dense satellite observations provides the opportunity for NRT monitoring of land disturbance. Coarse-resolution satellites (250–1000 m), such as Moderate Resolution Imaging Spectroradiometer (MODIS) and Visible Infrared Imaging Radiometer Suite (VIIRS), have been used for NRT monitoring of land disturbance due to their relatively high temporal frequency (Tang et al., 2019). For example, the operational system Terra-i (Reymondin et al., 2012) monitors deforestation for Latin America based on the 16-day composite of MODIS NDVI at 500-m resolution, and the FORMA alert system uses similar MODIS data and is capable of providing forest disturbance alerts every 16 days (Hammer et al., 2014). The Breaks For Additive Season and Trend (BFAST) monitoring method uses the 16-day MODIS NDVI composites at a 0.05° spatial resolution to monitor the drought-related disturbances (Verbesselt et al., 2012). Recently, the NRT-CCDC method (Tang et al., 2019) monitors forest disturbance using MODIS daily NDVI at a 250-m spatial resolution and has pushed the NRT monitoring further. However, the 250-m resolution satellite observations are not ideal for detecting anthropogenic disturbance that usually occurs at a scale much smaller than 250-m (Hansen and Loveland, 2012; Senf et al., 2017; Xin et al., 2013; Zhu and Qiu, 2022). The use of dense

* Corresponding author.
E-mail address: rongshang90@gmail.com (R. Shang).

https://doi.org/10.1016/j.rse.2022.113073
Received 30 July 2021; Received in revised form 5 March 2022; Accepted 1 May 2022
Available online 13 May 2022

satellite observations at a higher spatial resolution is critical and imperative for NRT monitoring of land disturbance (Senf et al., 2017).

The series of Landsat satellites can provide terrestrial observations at high spatial (30 m) and temporal (8-day revisit frequency) resolutions with two working satellites, making them ideal for obtaining fine-scale land disturbance information (Brown et al., 2019; Wulder et al., 2019; Zhu et al., 2020). Many approaches have been developed for detecting land disturbance based on Landsat time series, and their temporal frequencies are shifting from annual (Hansen et al., 2013; Hermosilla et al., 2015; Huang et al., 2010; Kennedy et al., 2010) to sub-annual scales (Brooks et al., 2014; Hamunyela et al., 2016; Hansen et al., 2016; Zhu et al., 2012; Zhu and Woodcock, 2014a). Though these sub-annual scale algorithms can update detection results with every new observation, they usually require a few months to collect sufficient consecutive observations to confirm a land disturbance, based on the assumption that noise is usually more ephemeral than land disturbances (Hamunyela et al., 2016; Zhu et al., 2015). To separate land disturbance from noises, the BFAST method requires 120–240 days (15 clear observations) to confirm a disturbance using Landsat time series in dry tropical forest (Hamunyela et al., 2016); the Continuous monitoring of Land Disturbance (COLD) algorithm needs at least 96 days to confirm a land disturbance (Zhu et al., 2020); the S-CCD approach requires at least 80 days to confirm forest disturbances using Landsat time series (Ye et al., 2021); and the GLAD forest alerts system requires 64 days to confirm forest loss using Landsat 7–8 time series (Hansen et al., 2016). Therefore, the time requirement of collecting continuous clear observations to separate land disturbances from noises could cause a substantial delay in land disturbance detection, and methods that could reduce this time requirement are of great interest.

Another major challenge in large-scale NRT monitoring of land disturbance is the huge amount of computation resources it requires, as even if the algorithm can provide NRT results, it can be delayed substantially by the required processing time (Zhu et al., 2020). Many algorithms require creating an unchanged reference to compare satellite observations in the detection of a land disturbance, and the speed of building the unchanged reference plays a major role in the algorithm's efficiency. For example, COLD updates the time series model based on all historical observations to predict the unchanged reference, and it requires 1000–3000 computing hours to process one Landsat Analysis Ready Data (ARD) tile (Zhu et al., 2020). For NRT monitoring across the CONUS, COLD would require one to three months to update the model estimation for every new observation if 500 cores were used for computation. High-performance computing (HPC) and cloud computing (CC) platforms have the potential to provide more computing capacity to reduce the processing delay. But these computing resources are still very expensive, and sometimes prohibitive. Some cloud computing platforms provide free accounts for non-commercial users (Gorelick et al., 2017), but have many limitations (e.g., the restricted programming framework, limited storage and processing time), making it difficult to run the more complicated algorithms designed for NRT land disturbance monitoring. Improving the efficiency of NRT land disturbance monitoring is therefore important for saving computing resources, energy, and money, and can help individuals who do not have good computing resources to conduct large-scale NRT monitoring of land disturbance.

The delay of NRT monitoring is referred to as time lag in this study, which is the delta days required for confirming a land disturbance after its first occurrence observed in satellite data. To obtain fine-scale land disturbance information in a timely fashion, the NRT monitoring algorithm should minimize the time lag without sacrificing the accuracy of NRT monitoring. Increasing the temporal frequency of high-resolution observations, reducing the number of needed consecutive observations to confirm land disturbances, and improving the time efficiency of the NRT monitoring algorithm are the three key directions to reduce the time lag and provide timely land change information.

To increase the temporal frequency of high-resolution observations, we will explore the use of four satellite sensors, including Landsat 7, Landsat 8, Sentinel-2A, and Sentinel-2B. Though Sentinel-2 can provide Landsat-like high-resolution observations, there are still large differences between Landsat and Sentinel-2 surface reflectance values, even for some harmonized datasets, such as the NASA harmonized Landsat and Sentinel-2 (HLS) data (Claverie et al., 2018; Shang and Zhu, 2019). Meanwhile, as far as we know, this is the very first time that all four sensors are used together for monitoring land change, as Landsat 7 data is usually ignored in the time series analysis due to the Scene Line Corrector (SLC)-off issue. For those studies that used both Landsat and Sentinel-2 data, most of them focused on a single type of land disturbance or disturbance within a single land cover/use type, such as burned area mapping (Roy et al., 2019), grassland change detection (Zhou et al., 2019), forest disturbance detection (Chen et al., 2021), dune migration mapping (Ding et al., 2020), and sugarcane plantation dynamics detection (Wang et al., 2020). Considering the importance of consistent time series data for change detection (Qiu et al., 2019), it is imperative to test methods that can provide more accurate harmonized Landsats 7–8 and Sentinel-2 data and use the full archive of this combined dataset for fine-scale land disturbance detection.

To reduce the number of required consecutive observations to confirm land disturbances, innovative methods that could better exclude outliers and can detect land disturbance based on higher thresholds without causing omission errors of land disturbances are needed. For example, some of the current Landsat-based disturbance algorithms, such as COLD (Zhu et al., 2020) and S-CCD (Ye et al., 2021), need at least six clear consecutive observations to confirm land disturbances, and new methods that require fewer consecutive observations to confirm land disturbances, such as four or five consecutive observations, could potentially reduce the lag time by 33.3% and 16.7%, respectively.

To increase the efficiency of the NRT algorithms, more efficient regression methods such as the online recursive regression could be a solution. The online recursive regression methods, such as Forgetting Factor, Kalman Filter, and Normalized Gradient, are able to update model parameters in an online mode based on newly collected observations and past coefficients much more efficiently than traditional regression methods (Khalil and Dombre, 2004). As most online regression methods do not need to host all historical data, it is possible to run NRT algorithms at a large scale without the need for massive data storage. The S-CCD approach incorporated the Kalman Filter based method in its online model estimation and achieved up to ~4.4 times speedup for computation against the COLD algorithm (Ye et al., 2021), which is a nice attempt to use online estimation in change detection, but it is only designed for detecting forest disturbance and still needs more than 80 days to confirm a change. Therefore, it is of great interest and importance to develop a more efficient NRT monitoring approach for detecting all land disturbance types with a shorter delay.

In this study, we aim to propose a novel approach for Near-Real-Time MOnitoring of laNd dIsturbance based on Time-series of harmOnized Reflectance (NRT-MONITOR) from Landsats 7–8 and Sentinel-2 data at a 30-m spatial resolution. The NRT-MONITOR approach can substantially reduce the time lag of land disturbance monitoring at similar accuracies of other state-of-the-art algorithms, and is capable of providing land disturbance alerts with a land disturbance probability every three days.

2. Data and study area

2.1. Harmonizing Landsats 7–8 and Sentinel-2 data

The harmonized Landsats 7–8 and Sentinel-2 data at the Blue, Green, Red, Near-Infrared (NIR, Band 8A for Sentinel-2), Shortwave Infrared 1 (SWIR1), and 2 (SWIR2) bands were used to develop and evaluate the NRT-MONITOR algorithm. Landsat 8 (Collection 1) and Sentinel-2 surface reflectance data at a 30-m spatial resolution were downloaded from the NASA Harmonized Landsat 8 and Sentinel-2 (HLS) V1.4 product (Claverie et al., 2018), and Landsat 7 (Collection 1) surface reflectance data was preprocessed and downloaded from Google Earth Engine (GEE) (Gorelick et al., 2017). The processing of Landsat 7 includes the Bidirectional Reflectance Distribution Function (BRDF) correction using the c-factor approach (Roy et al., 2016), re-projection, and clipping from Landsat WRS-2 (Worldwide Reference System-2) to the Sentinel-2 MGRS (Military Grid Reference System) tile with nearest neighbor resampling. The Quality Assessment (QA) band created from the Fmask algorithm was used for the identification of clear observations (Zhu et al., 2015; Zhu and Woodcock, 2012).

We applied the newly developed Time-series-based Reflectance Adjustment (TRA) approach (Shang and Zhu, 2019) to reduce the reflectance difference among Sentinel-2, Landsat 7, and Landsat 8 with Landsat 8 data as the reference for this new reflectance adjustment approach. Without the adjustment, the reflectance difference (mostly caused by bandpass difference) between different sensors will influence the detection of land disturbance in two aspects (Fig. 1): (i) higher commission errors, where the reflectance difference from the sensors is detected as a land disturbance event; (ii) higher omission errors, where the signal of a true land disturbance event is buried in the reflectance difference between sensors. To minimize the influence of reflectance difference on land disturbance monitoring, we modified the original TRA approach in three aspects: First, the TRA approach would only be applied if the mean reflectance difference between two sensors is large enough (> 0.002) to cause trouble in change detection. Second, to reduce the influence of noise on the built relationship for the reflectance adjustment, the linear regression using the ordinary least squares was replaced by a robust regression using iteratively reweighted least squares with a bi-square weighting function, which can assign lower weights to the outliers by the iterative reweighting process. Third, the slope of the built linear relationship for the reflectance adjustment was limited to a realistic range (e.g. between 0.8 and 1.2). If the slope is outside this range, 5% of the matched observation pairs departed far from the initial linear relationship will be removed and the remaining will be used to rebuild the linear relationship. This process will be iteratively performed until the slope is within the range.

The remaining outliers missed by Fmask or the QA of the HLS product, such as clouds, cloud shadows, and snow/ice, in the time series should be well screened before land disturbance monitoring. Unlike using a complicated algorithm such as Tmask (Zhu and Woodcock, 2014b), a simple time series filter was used to remove the remaining outliers (e.g., clouds and cloud shadows) in the time series of all four sensors after the reflectance adjustment:

$$\sum_{\Lambda=1}^{k}\left[\frac{\rho_{\Lambda}(i)-0.5\times(\rho_{\Lambda}(i-1)+\rho_{\Lambda}(i+1))}{D_{\Lambda}(i)}\right]^{2}>\chi^{2}(kNp) \tag{1}$$

$$D_{\Lambda}(i)=\sqrt{\sum_{j=2}^{N-1}[\rho_{\Lambda}(i)-0.5\times(\rho_{\Lambda}(i-1)+\rho_{\Lambda}(i+1))]^{2}\Big/(N-2)} \tag{2}$$

where, k is the number of bands, Λ is the band index (from 1 to k), $\rho_{\Lambda}(i)$ is the ith observation, N is the number of observations, Np is the probability of an outlier, and $\chi^2(k, Np)$ is the threshold used for the outlier removal derived from the chi-squared distribution. Outliers usually alter surface reflectance abruptly but are much more ephemeral than a real land change signal (Zhu et al., 2020). Therefore, they can be removed by comparing reflectance to the mean reflectance of its nearby two observations. The optimal probability for outlier screening is 0.99 (see Fig. S1 for details).

2.2. Reference data and study area

A total of 1200 reference samples from 2015 to 2019 were randomly selected from four HLS tiles, in which each tile has 300 randomly selected reference samples (Fig. 2). The four HLS tile IDs are T10SFG, T13TCF, T18TXM, and T19TDL. Tile T10SFG is selected because of the

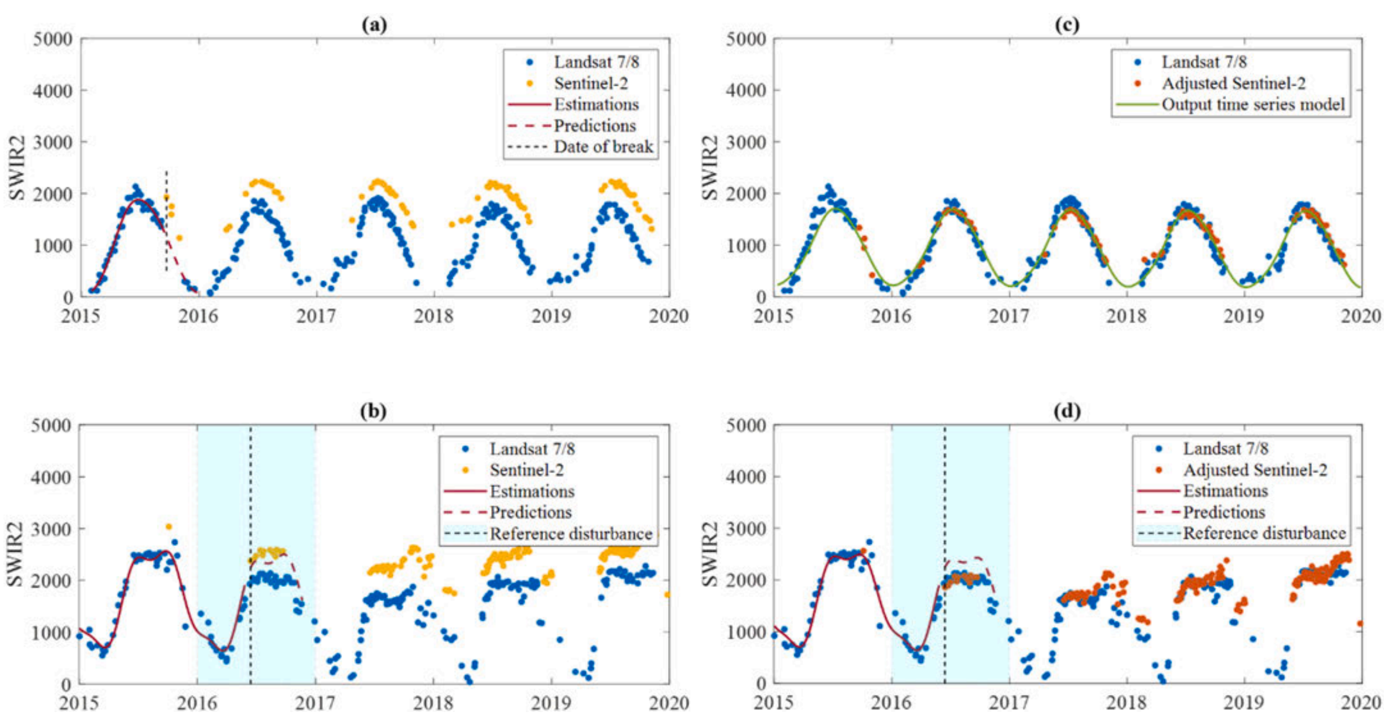

Fig. 1. Two typical examples of land disturbance monitoring before (a-b) and after (c-d) reflectance adjustment between Landsat 7/8 and Sentinel-2 surface reflectance data. (a) shows a commission error where the reflectance difference between Landsat and Sentinel-2 data is misidentified as a land disturbance event; (b) shows an omission error where the signal of a true land disturbance event is missed by the land disturbance monitoring algorithm due to the large reflectance difference between Landsat and Sentinel-2 data; (c) shows that the commission error is corrected after applying the reflectance adjustment for the first example (a) with no land disturbance; (d) shows that the omission error is corrected after applying the reflectance adjustment for the second example (b) with a land disturbance occurred in 2016. The "Reference disturbance" in the second example refers to the interpreted land disturbance in the reference data.

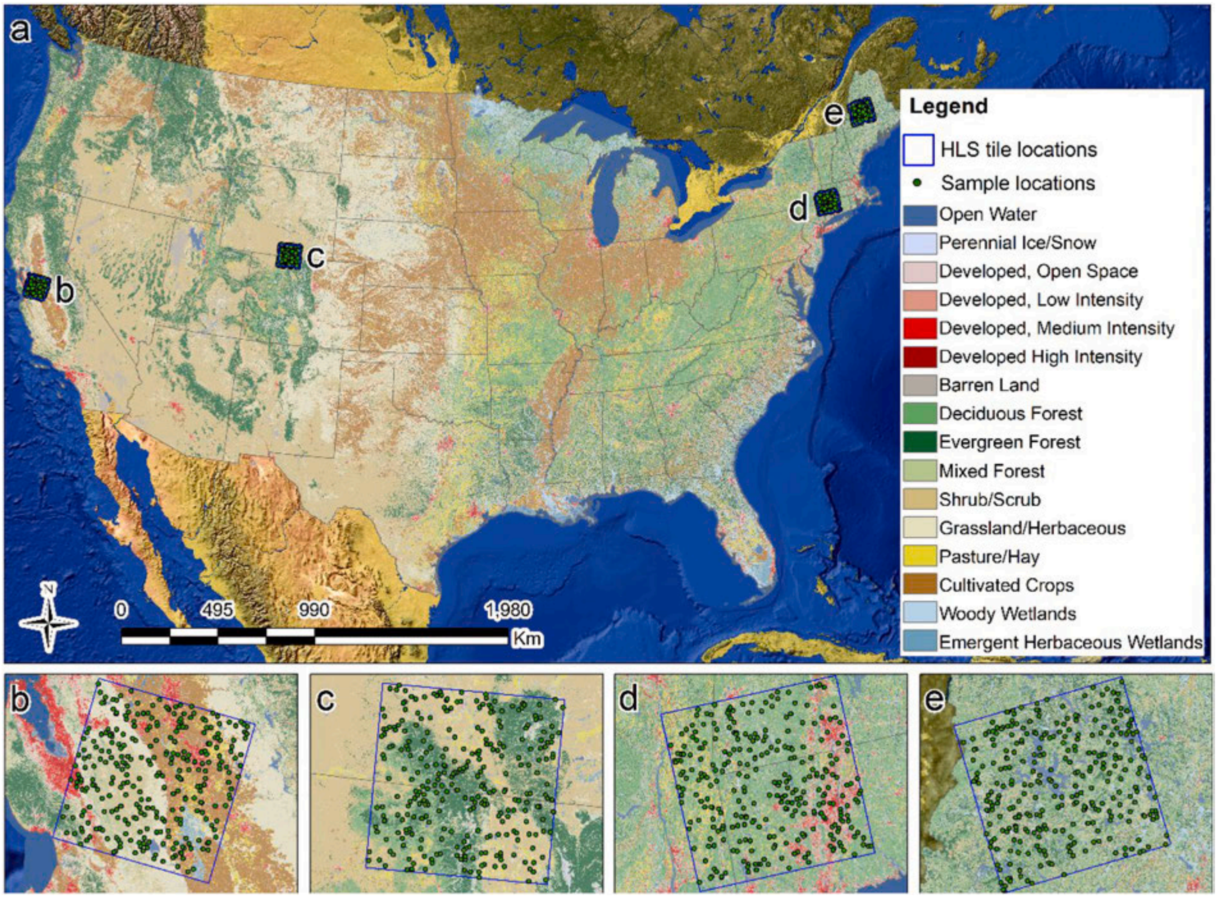

Fig. 2. Spatial distribution of the 1200 Landsat reference samples (green circles) overlaid on the NLCD 2011 land cover (Homer et al., 2015) map (a) and the enlarged figures (b-e) for four HLS tiles (T10SFG, T13TCF, T18TXM, and T19TDL). (For interpretation of the references to color in this figure legend, the reader is referred to the web version of this article.)

high occurrences of land disturbances from fire and mechanical, and it includes the land cover types of cultivated crops, developed, forest, shrubs, and grasslands. Tile T13TCF is selected because of the high occurrences of land disturbances from stress and fire, and it mainly includes the land cover types of forest and shrubs. Tile T18TXM is selected because of the high occurrences of land disturbances from wind and harvest, and it mainly includes the land cover types of forest and developed. Tile T19TDL is selected because of the high occurrences of land disturbances from hydrology and harvest, and it mainly includes the land cover types of forest and open water. All reference samples were interpreted based on the time series visualization and disturbance data collection software – TimeSync (Cohen et al., 2010) with the help of Google Earth high-resolution images, where all available Landsats 7–8 and Sentinel-2 images were incorporated to obtain the accurate date of land disturbance. These reference samples include many kinds of land disturbance types such as harvest, fire, stress, wind, mechanical, and hydrology, and 2.3% of reference samples had more than one land disturbance event from 2015 to 2019.

3. Methods

3.1. The NRT-MONITOR algorithm

The NRT-MONITOR algorithm can monitor land disturbance in near-real-time with or without historical detection results. Fig. 3 shows the flowchart of NRT-MONITOR, which consists of four major steps: obtaining the initial model parameters (Section 3.1.1), estimating the time series combined from the stored historical and new observations using the Forgetting Factor recursive regression (Section 3.1.2), NRT monitoring and confirming a land disturbance (Section 3.1.3), and processing the end of time series for future NRT monitoring (Section 3.1.4). Before confirming a land disturbance, a "break" is used to indicate spectral changes that deviate from recursive estimations, and each "break" separates the time series into two "time segments". The optimal thresholds used in NRT-MONITOR are summarized in Table 1, and the detailed descriptions of the parameters could be found in Sections 3.1.1–3.1.4.

3.1.1. Obtain the initial model parameters

The harmonic time series model with 3 harmonic items (Eq. (3)) was used to model the time series of surface reflectance. This model was selected because it was widely used for change detection (Brooks et al., 2014; Hamunyela et al., 2016; Verbesselt et al., 2012; Zhang et al., 2021; Zhu et al., 2020; Zhu and Woodcock, 2014a). The Green, Red, NIR, SWIR1, and SWIR2 bands were selected for NRT land disturbance monitoring because they were demonstrated to be the optimal band combinations for detecting land disturbance (Zhu et al., 2020).

$$y(t,\Lambda) = a(\Lambda) + b(\Lambda)t + \sum\nolimits_{k=1}^{3}\left[c(k,\Lambda)cos\left(\frac{2k\pi}{T}t\right) + d(k,\Lambda)cos\left(\frac{2k\pi}{T}t\right)\right] \quad (3)$$

where, $y(t,\Lambda)$ is the estimated surface reflectance; t is the date; Λ is the Landsat band; k is the frequency of harmonic component (1, 2, and 3); T is the number of days per year (365.25); $a(\Lambda)$, $b(\Lambda)$, $c(1,\Lambda)$, $d(1,\Lambda)$, $c(2,\Lambda)$, $d(2,\Lambda)$, $c(3,\Lambda)$, and $d(3,\Lambda)$ are the model parameters. The initial model parameters are critical for starting the recursive regression, and we will use the time series model estimated in the last time segment in

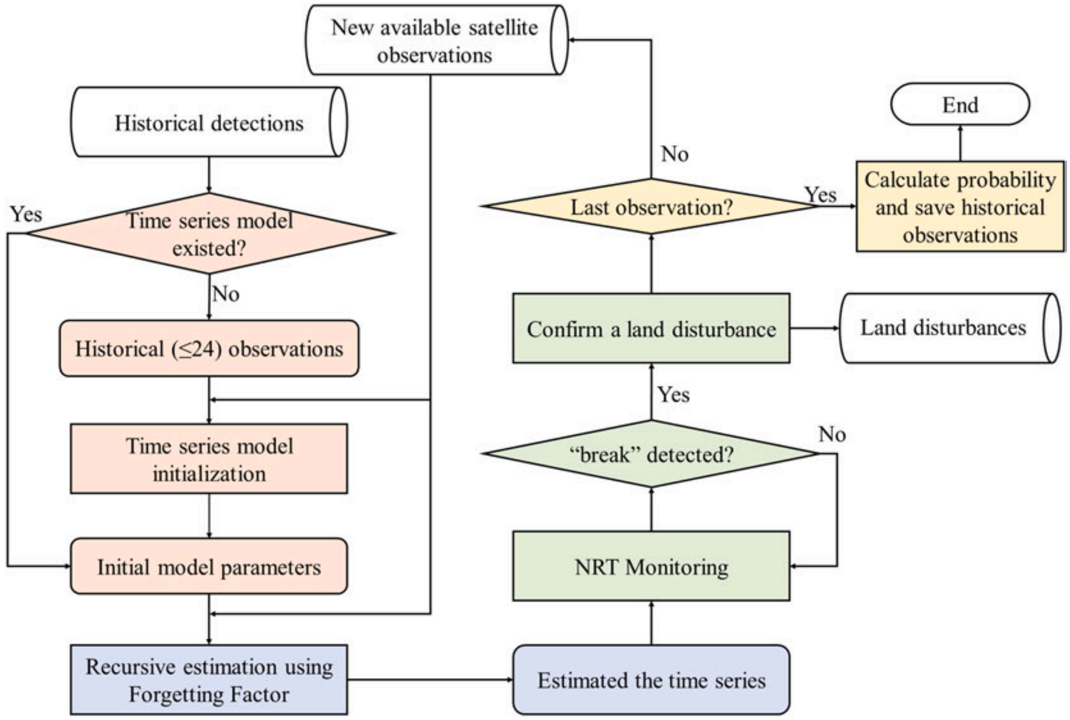

Fig. 3. The flowchart of the NRT-MONITOR algorithm. The four colors of light red, light blue, light green, and yellow indicate four major steps of the NRT-MONITOR algorithm: light red is for obtaining the initial model parameters, light blue is for estimating the time series using Forgetting Factor based recursive regression, light green is for NRT monitoring and confirming a land disturbance, and light yellow is for processing the end of time series for future NRT monitoring. The "break" is used to indicate spectral changes that deviate from recursive estimations. (For interpretation of the references to color in this figure legend, the reader is referred to the web version of this article.)

Table 1
The optimal thresholds used in the NRT-MONITOR algorithm. RMSE: root mean square error between satellite observations and algorithm estimations.

Parameter	Threshold	Sensitive analysis
The threshold for outlier removal	0.99	Fig. S1
Forgetting parameter	0.999	Fig. S2
Number of modeled observations to stabilize recursive regression	120	Fig. S3
Minimum number of consecutive observations for confirming a land disturbance	4	Fig. S4
Time interval of the RMSE look-up-table	8 days	Fig. S6
Minimum number of observations required for calculating RMSE	24	Fig. S7
The minimum time interval for confirming a land disturbance	30 days	Fig. 6
The change threshold used for land disturbance detection	0.99999	Fig. 6

historical detections if they already exist. If there are no previous time series model coefficients estimated, we will follow the same model initialization procedure as COLD in our model initialization (Zhu et al., 2020). This procedure used the first part of time series to detect the stable period with a stability test (Zhu et al., 2020):

$$|L_{slope}| + max\{|L_{start}|, |L_{end}|\} \langle T_{CT} \tag{4}$$

where, $|L_{slope}|$ is the change magnitude from the slope of time series, $|L_{start}|$ is the change magnitude of the first observation, $|L_{end}|$ is the change magnitude of the last observation, and T_{CT} is the change threshold (seeing Section 3.1.3 for details). When it passed the stability test, a time series model will be initiated, and its model parameters will be used as the initial model parameters.

3.1.2. Estimate the time series using forgetting factor based recursive regression

Improving the time efficiency and reducing the storage demand are critical issues that need to be addressed for large-scale monitoring of land disturbance. We used the online recursive estimation algorithm (Carlson, 1973; Khalil and Dombre, 2004) to solve both issues as shown in Eq. (5).

$$\hat{\theta}(t) = \hat{\theta}(t-1) + K(t)(y(t) - \hat{y}(t)) \tag{5}$$

where, $\hat{\theta}(t)$ is the parameter estimate at time t; $y(t)$ is the observed output at time t; $\hat{y}(t)$ is the prediction of $y(t)$ based on observations up to time t-1; $K(t)$ is the gain, which determines how much the current prediction error $y(t) - \hat{y}(t)$ affects the update of the parameter estimate.

The gain $K(t)$ is the most critical component in the algorithm and is shown in Eq. (6).

$$K(t) = Q(t)\psi(t) \tag{6}$$

where, $\psi(t)$ represents the gradient of the predicted model output $\hat{y}(t|\theta)$ concerning the parameters θ; $Q(t)$ is the parameter and there are three mathematical approaches for its derivation including Forgetting Factor, Kalman Filter, and Unnormalized Gradient (Carlson, 1973; Khalil and Dombre, 2004). Linear regression is used to calculate the gradient $\psi(t)$ as shown in Eq. (7).

$$y(t) = \psi^T(t)\theta(t) + e(t) \tag{7}$$

where, $\psi(t)$ is the regression vector that is computed based on previous values of measured inputs and outputs, and $e(t)$ is the noise. Experiments using the three mathematical approaches with their default settings showed that the Forgetting Factor could present a large difference between the estimated values and real observations when a land change occurred (Fig. 4). Therefore, the Forgetting Factor was used to estimate $Q(t)$.

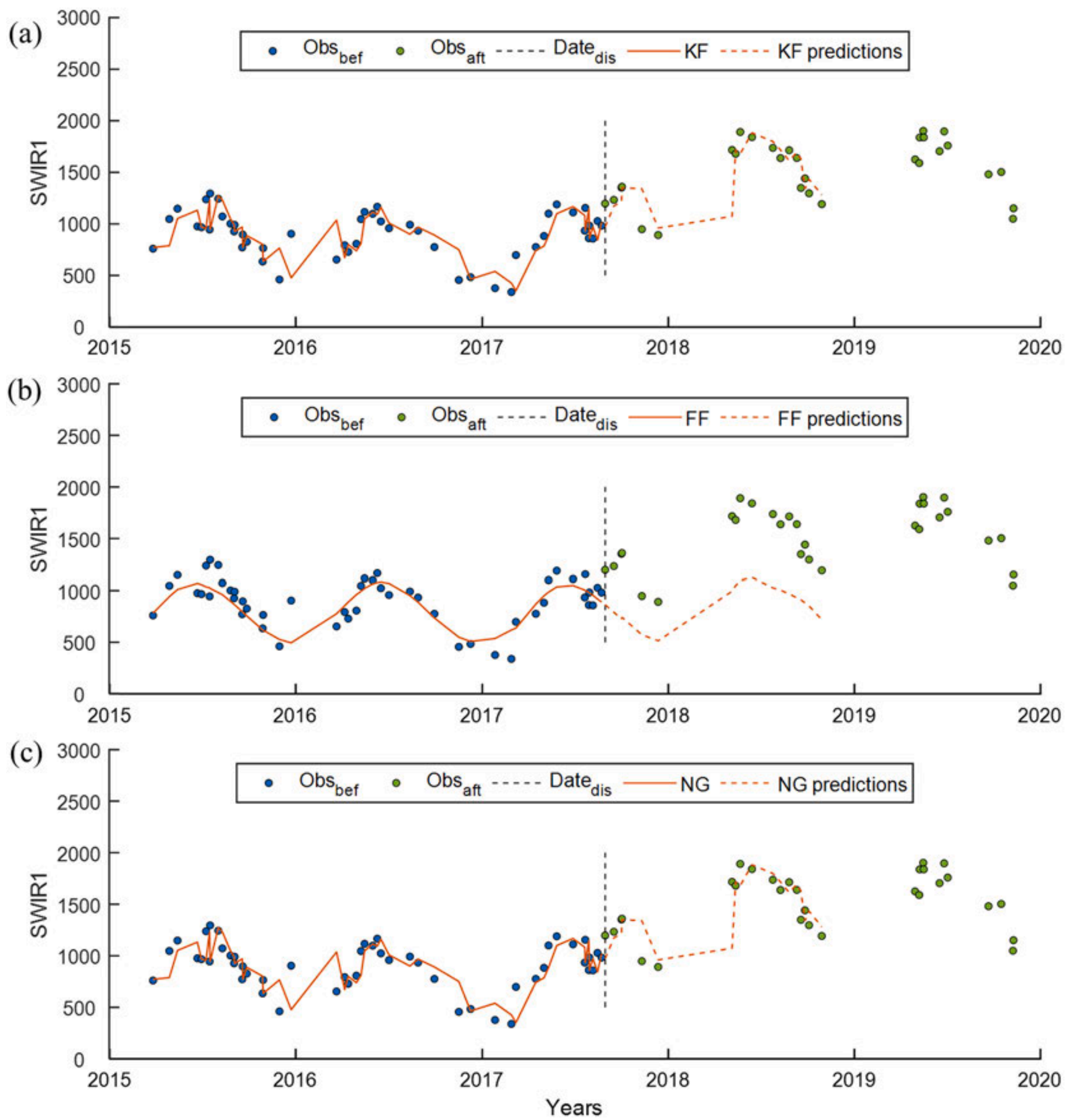

Fig. 4. Example of SWIR1 band (×10,000) surface reflectance estimations from Forgetting Factor, Kalman Filter, and Normalized Gradient algorithms with their default MATLAB settings of the parameters for a pixel that has undergone a land disturbance in 2017. Obs$_{bef}$: Observations before land disturbance; Obs$_{aft}$: Observations after land disturbance; Date$_{dis}$: Date of land disturbance; KF: Kalman Filter; FF: Forgetting Factor; NG: Normalized Gradient. Note that both Kalman Filter and Normalized Gradient respond to the change of the time series closely, while it takes quite some time for Forgetting Factor to respond to this change. This unique latency from Forgetting Factor makes it capable of detecting land disturbance based on the difference between estimated values and the actual remote sensing observations.

$$Q(t) = P(t-1)\Big/\left(\lambda + \psi^T(t)P(t-1)\psi(t)\right) \tag{8}$$

$$P(t) = \frac{1}{\lambda}\left(P(t-1) - \frac{P(t-1)\psi(t)\psi^T(t)P(t-1)}{\lambda + \psi^T(t)P(t-1)\psi(t)}\right) \tag{9}$$

where, $P(t)$ is the covariance, and λ is the forgetting parameter between 0 and 1. The forgetting parameter discounts historical observations exponentially, and $1/(1-\lambda)$ represents the memory horizon of the Forgetting Factor. We tested 5 different values (e.g., 0.9, 0.95, 0.99, 0.999, and 0.9999) for the forgetting parameter, and 0.999 was determined as the optimal threshold (Fig. S2).

The initial recursive regressions based on the Forgetting Factor are critical for stabilizing the recursive estimations of surface reflectance. The remaining clouds, cloud shadows, or other outliers at the beginning of the time series can influence the initial recursive regressions which may negatively impact the land disturbance detection. To minimize these impacts, we proposed a novel method that adds a short period of modeled observations ahead of the time series to start recursive regression. The modeled observations were derived from the harmonic time series model using the initial model parameters with a time interval of 8 days. The 8 days is chosen because it is the revisit days of two Landsat satellites. Adding modeled observations will influence how the Forgetting Factor recursive regression follows the historical trajectory. The more model observations are used, the more accurate the estimates from the recursive regression, and the less the impact of remaining outliers at the beginning of the time series. We tested the impact of using different numbers of modeled observations on stabilizing the Forgetting Factor recursive regression. Without using modeled observations (Fig. 5a), the estimations could follow the "false" trends caused by remaining outliers that were estimated in the first year and negatively impact model capability for land disturbance monitoring. The impact of these outliers is reduced when using 30 modeled observations (Fig. 5b), and it is minimized when using 120 modeled observations (Fig. 5c). The sensitive analysis determined 120 modeled observations as the optimal threshold to achieve the highest monitoring accuracy of land disturbance (Fig. S3).

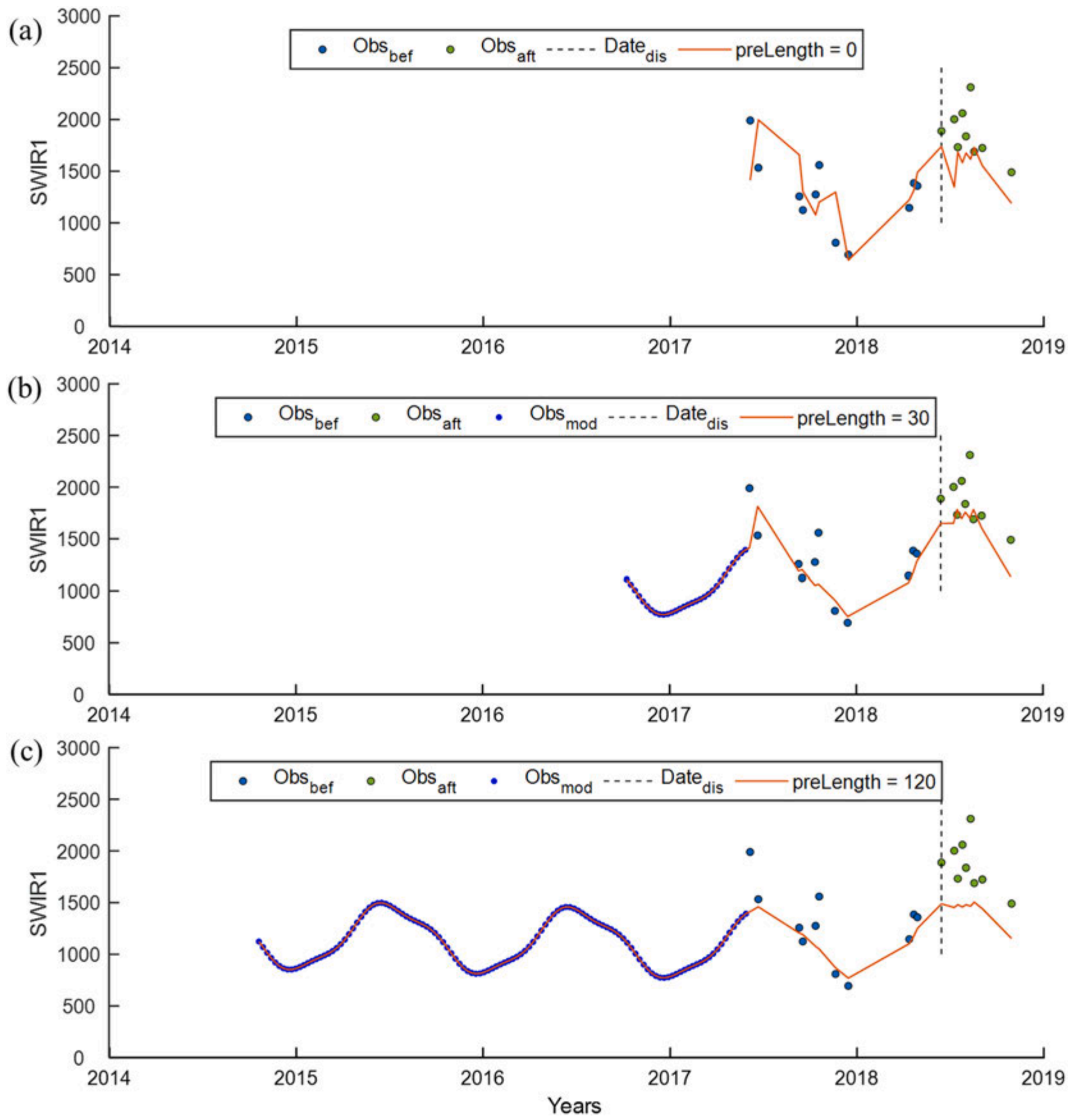

Fig. 5. Example of using the modeled observations to stabilize the recursive regression at the SWIR1 band (×10,000). (a) No modeled observations; (b) 30 modeled observations; and (c) 120 modeled observations. Obs_{bef}: Observations before land disturbance; Obs_{aft}: Observations after land disturbance; $Date_{dis}$: Date of land disturbance; Obs_{mod}: Modeled observations; preLength: The number of modeled observations.

3.1.3. NRT monitoring and confirming a land disturbance

NRT monitoring starts when the recursive estimation is completed, and it searches the change signal ("break") from the start to the end of the merged time series (historical plus new observations). It is worth noting that historical observations are only needed when there is no historical time series model and there are no more than 24 historical observations saved in the previous monitoring procedure (see Section 3.1.4 for details). There are three major processes in NRT monitoring: (i) detecting a "break", (ii) recording time segments, and (iii) moving forward. If no "break" is detected for the current observation, the procedure will move forward to the next observation in the time series. If a change signal is identified at the *i*th observation (defined as *i_break*) in the time series, the time segment from the first to *i_break-1* of time series will be estimated by the harmonic time series model. The model parameters, change magnitudes, and some other parameters (see Table S1 for details) will be saved for the use of recursive regression and disturbance agent classification. In this study, we only focus on monitoring land disturbance, and the classification of land disturbance agents is not included.

A land disturbance is confirmed by measuring the differences between the satellite observations and algorithm estimations, as well as the duration of these differences. The difference is calculated by a normalized change magnitude (CM) derived from the five spectral bands and a change threshold based on the chi-squared distribution (Eq. (10)).

$$CM(i) = \sum_{\Lambda=1}^{k} \left(\frac{y_{\Lambda}(i) - y_{\Lambda}'(i)}{RMSE_{\Lambda}(i)} \right)^2 \quad (10)$$

$$RMSE_{\Lambda}(i) = \sqrt{\sum_{j=1}^{N} \left(y_{\Lambda}(i) - y_{\Lambda}'(i)\right)^2 \Big/ N} \quad (11)$$

where, k is the total number of detecting bands, Λ is the band index (from 1 to k), $y_{\Lambda}(i)$ is the i^{th} observation, $y_{\Lambda}'(i)$ is the i^{th} model prediction in the time series, N is the total number of observations used for calculating RMSE (see supplementary material and Fig. S5-S7 for details), and j is the observation index (from 1 to N). The calculation of RMSE is critical for monitoring land disturbance. The Day-of-year (DOY)-nearest observations were suggested to calculate RMSE because they can describe seasonal changes in RMSE (Zhu et al., 2020), but it is a challenge to select the DOY-nearest observations without saving all historical observations. To calculate seasonally dynamic RMSE for NRT land disturbance monitoring, we used a look-up table (LUT) to store the sum of square errors and the number of observations used in calculating RMSE. Fig. S5 shows the schematic diagrams on how to calculate RMSE for a target observation: first transfer the acquisition dates of all previous observations into DOYs, then divides these observations into different bins using a bin width (e.g. 8, 16, 24, or 32 days) according to their DOYs, and last uses a LUT to store the sum of square errors and the number of observations within each bin for updating RMSE. If the number of observations within a bin is smaller than a threshold, the observations in their neighboring bins will be added to calculate RMSE. Sensitive analysis indicates that the optimal bin width is determined as 8 days (Fig. S6) and the optimal number of observations used in the RMSE calculation is determined as 24 (Fig. S7).

The duration of the differences is measured by integrating a minimum time interval and a minimum number of consecutive observations. The minimum time interval, which is defined as the minimum days that a land disturbance lasts, is integrated to consider the variability of temporal frequency in the harmonized time series for NRT monitoring, where large changes in temporal frequency could influence land disturbance detection (Brown et al., 2019). Another advantage of integrating a minimum time interval is the improved spatial and temporal consistency of the detected land disturbance (Ye et al., 2021). Using these indicators, a land disturbance is determined in Eq. (12).

$$\begin{aligned} & min\{CM(i), CM(i+1), \ldots, CM(i+N_{min}-1)\} \\ & \geq \chi^2(k, T_{CT})\ and\ t(i+N_{CO}-1) - t(i) \geq D_{min} \end{aligned} \tag{12}$$

where, k is the total band numbers, N_{min} is the minimum number of consecutive observations, $CM(i)$ is the change magnitude, T_{CT} is the change threshold, $\chi^2(k, T_{CT})$ is the normalized threshold derived from the chi-squared distribution, $t(i)$ is the date, and D_{min} is the minimum time interval. The minimum number of consecutive observations was determined to be 4 in the sensitive analysis (Fig. S4). Sensitive analysis was also conducted using different minimum time intervals and change thresholds (Fig. 6). The optimal parameters for NRT land disturbance monitoring include a minimum of four consecutive observations, a minimum time interval of 30 days, and a change threshold of 0.99999 based on the harmonized Landsats 7–8 and Sentinel-2 data. It is worth noting that “breaks” contributed from the vegetation regrowth are excluded from land disturbance following the same procedure used in COLD (Zhu et al., 2020) if the time series model after the “break” could be estimated.

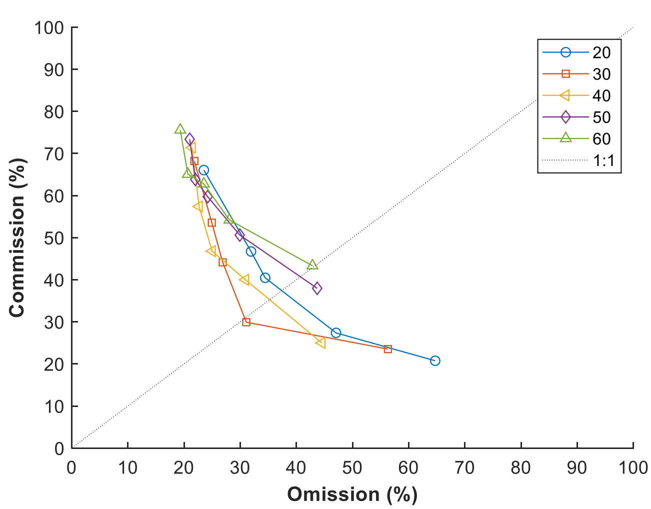

Fig. 6. Land disturbance monitoring accuracies with different time intervals from 20 to 60 days based on the harmonized Landsats 7–8 and Sentinel-2 time series. Five points in each curve represent change thresholds of 0.999, 0.9999, 0.99995, 0.99999, and 0.999999, respectively.

NRT-MONITOR can also provide land disturbance alerts with a probability map before changes are fully confirmed. The disturbance probability is calculated as the ratio between the number of changed observations (N_C) and the minimum number of consecutive observations (N_{min}) to confirm a change or the ratio between the time interval of first and current changed observations (D_C) and the minimum time interval to confirm a change (D_{min}), whichever is smaller (Eq. (13)).

$$P = min(N_C/N_{min}, D_C/D_{min}) \times 100\% \tag{13}$$

3.1.4. *Processing the end of time series for future NRT monitoring*

The end of the time series needs special processes to prepare for future NRT monitoring. There are four scenarios as shown in Fig. 7: (1) Scenario 1: no disturbance is observed before the end of time series; (2) Scenario 2: a disturbance is confirmed and the last time segment has ≥24 clear observations; (3) Scenario 3: a disturbance is confirmed but the last time segment has <24 clear observations; (4) Scenario 4: the time series end with an unconfirmed disturbance. The threshold of 24 clear observations is used because it is one of the basic requirements for time series model initialization (Zhu et al., 2020). For Scenarios 1–2, there is a time series model estimated for the time segment extended to the end of time series, and the model parameters will be saved for future monitoring; For Scenario 3, we cannot estimate time series models for the last time segment due to lack of observations, and all observations (<24) within this time segment will be saved for future time model initialization; For Scenario 4, the disturbance has not been fully confirmed, and the latest 24 clear observations will be saved to update the land disturbance monitoring in the future.

3.2. *Algorithm performance evaluation*

The commission error, omission error, and F1 score were chosen for accuracy assessment (Zhu et al., 2020). Commission error describes the land disturbances that are only detected by the algorithm but are not labeled as land disturbances in the reference data. Omission error depicts the land disturbances recorded in the reference data but is not detected by the algorithm. F1 score provides a balance between the commission and omission errors. The reference land disturbance samples were randomly separated into two parts: 50% were used for algorithm development (hereafter will be called calibration samples), and the remaining 50% were used for accuracy assessment (hereafter will be called validation samples). To get a more robust estimation of accuracy, we performed the accuracy assessment eight times with different random selections (50%) of the validation samples, and their mean values and one standard deviation (95% confidence interval) of commission error, omission error, and F1 score were used to quantify the final NRT monitoring accuracy. Every land disturbance event in the reference plots would be evaluated, and the agreement of a disturbance event can be confirmed if the detection and the reference are correct both in space and time.

Since the temporal coverage of the reference samples is all historical years, we assumed that observations at each one-year period are “future observations”, and then run the NRT-MONITOR algorithm based on these “future observations” and the disturbance detection results ended at the end of each previous year. The total validation periods from 2015 to 2019 were separated into five one-year monitoring periods, and the average accuracy of all five periods would be regarded as the final accuracy. This validation procedure could also be used for evaluating the accuracy of land disturbance alerts provided at different land disturbance probabilities.

4. Results

4.1. *Monitoring land disturbance*

The NRT-MONITOR algorithm can monitor land disturbance when

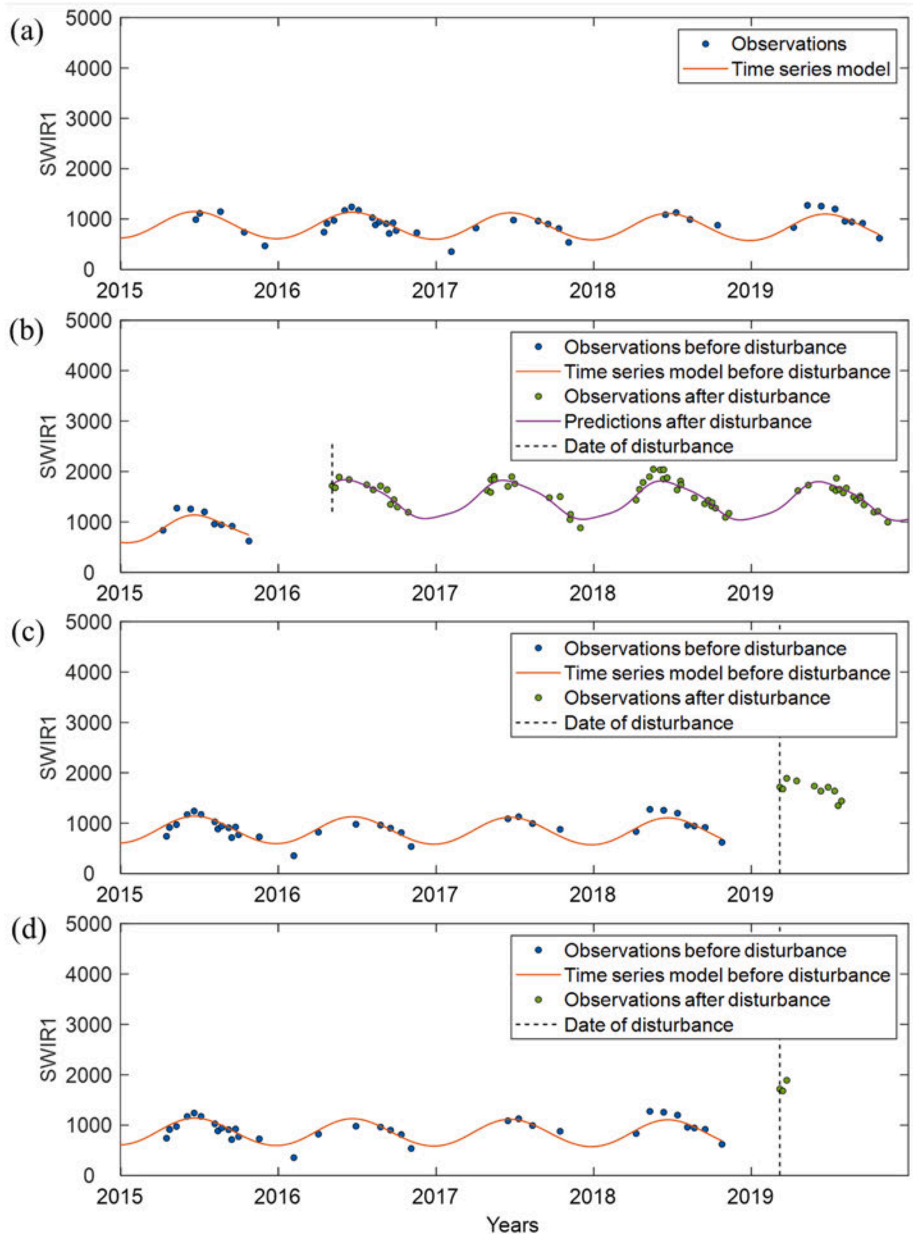

Fig. 7. Four scenarios of disturbance monitoring at the end of SWIR1 band (×10,000) time series: (a) no disturbance is observed, (b) a disturbance is confirmed and the last time segment has ≥24 clear observations, (c) a disturbance is confirmed but the last time segment has <24 clear observations, and (d) the time series end with an unconfirmed change.

new satellite observations are available. By assuming historical observations as "future observations", NRT-MONITOR was tested by updating the land disturbance monitoring annually. Fig. 8 shows the updated monitoring of land disturbances in each year from 2014 to 2018 for a subset of the HLS tile T19TDL. Landsat 8 false-color composite (R: SWIR1, G: NIR, B: R) images obtained on July 21th, 2013 (Fig. 8a) and September 26th, 2020 (Fig. 8d) are shown as a comparison. Fig. 8b-c, Fig. 8e-f, and Fig. 8h-i show the enlarged views of the red squares labeled in Fig. 8a, Fig. 8d, and Fig. 8g, respectively. The spatial distribution of the detected land disturbances from NRT-MONITOR was similar to the clear-cut areas in the false-color composite images, and there were only small differences that could be observed for some small patches. The results for the HLS tiles T10SFG and T18TXM are shown in Fig. S8 and Fig. S9 (the tile T13TCF is not included because it was selected as an example for providing alerts of potential land disturbance in Fig. 10), and land disturbances types, such as harvest, stress, fire, mechanical, and hydrology, can be well captured by NRT-MONITOR. Fig. 9 shows the NRT-MONITOR land disturbance monitoring results for a single year (2015, 2016, or 2017) at different locations (Fig. 9b-h), in which the colors represent the DOYs the land disturbances are detected.

4.2. Alerting potential land disturbances

NRT-MONITOR can be integrated into an alerting system to capture potential land disturbances with a disturbance probability map that is updated every three days based on the harmonized Landsats 7–8 and Sentinel-2A/B observations. Fig. 10 shows the NRT updated potential land disturbance (e.g., forest fire) maps derived from NRT-MONITOR at the border of Wyoming state and Colorado state (selected from the HLS tile T13TCF). This forest fire burned intermittently for more than two months from June 21st to September 9th, 2016. There were 28 images

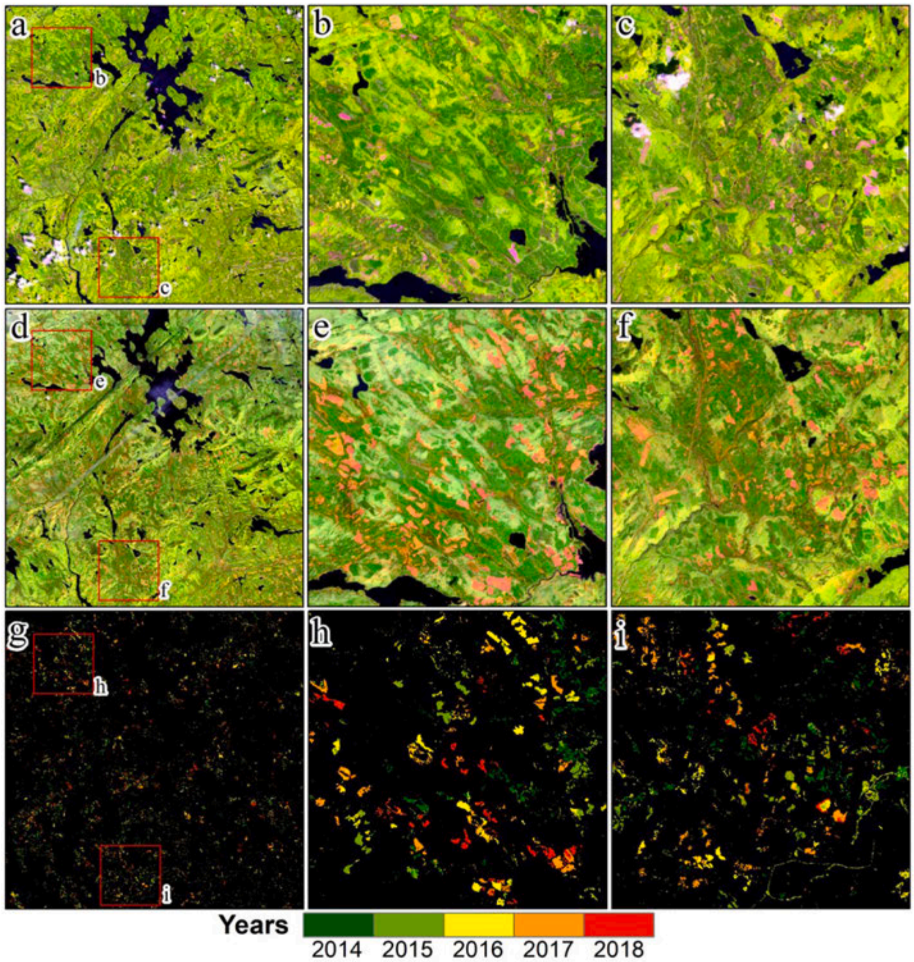

Fig. 8. The false-color composite images (a-f) and the updated land disturbance maps (g-i) generated by NRT-MONITOR from 2014 to 2018 for a subset of the HLS tile T19TDL. (a-c) The false-color composites (R: SWIR1, G: NIR, B: R) are Landsat 8 images collected on July 21st, 2013. (d-f) The false-color composites (R: SWIR1, G: NIR, B: R) are Landsat 8 images collected on September 26th, 2020. (b-c), (e-f), and (h-i) are the enlarged views of red squares labeled in (a), (d), and (g), respectively. (For interpretation of the references to color in this figure legend, the reader is referred to the web version of this article.)

obtained from Landsat 7, 8, and Sentinel-2A/B during this period (Table S2), and the average revisit cycle was 2.96 days. To avoid redundancy, we only select several key dates to show the updated probability maps of the land disturbance. The burning fires were captured on June 21st, June 26th, July 9th, July 14th, July 21st, July 23th, July 29th, July 30th, and August 15th. With the newly collected observations, the previously burned areas were updated with a higher land disturbance probability, and the newly burned areas were also captured with a relatively low land disturbance probability. Although data gaps from Landsat-7 SLC-off, fire smokes, clouds, and cloud shadows affected the spatial distribution of land disturbance probabilities to a certain extent, the spatial patterns of the fire expansion were still well-captured. The noises were sometimes detected with a low land disturbance probability and later removed if the updated land disturbance probabilities could not reach 100% in the future.

4.3. The time lag of NRT monitoring

The time lag is one of the key indicators to evaluate the NRT land disturbance monitoring. Fig. 11 shows the mean time lags of the NRT land disturbance monitoring by NRT-MONITOR based on the harmonized Landsats 7–8 and Sentinel-2 time series for each year. Though NRT-MONITOR only needs four clear consecutive observations to confirm a land disturbance, the statistics of using six clear consecutive observations to confirm a land disturbance were also included as a comparison as this value was used in the COLD and S-CCD algorithm. The statistics of not using the minimum time interval (Fig. 11a) were also added to evaluate its influence on the time lags. The mean time lags were 27 $\pm$ 19 days and 48 $\pm$ 28 days using four and six clear consecutive observations based on the harmonized Landsats 7–8 and Sentinel-2 data, respectively. Due to changes in the observing frequency with the launch of Sentinel-2A in 2015 and Sentinel-2B in 2017, the mean time lags showed a decreasing trend from 2015 to 2017. When using a minimum time interval of 30 days (Fig. 11b), the mean time lags increased to 35 $\pm$ 14 days and 50 $\pm$ 26 days using four and six consecutive observations, respectively. These results indicated that NRT-MONITOR could still provide 25–33% faster confirmation (35 days vs 50 days) of land disturbance than the COLD and S-CCD algorithms even if the harmonized Landsats 7–8 and Sentinel-2 data is used as input for all algorithms being compared. This improvement in confirmation speed comes from reducing six clear consecutive observations to four without sacrificing the NRT monitoring accuracy in NRT-MONITOR. It is worth noting that reducing the number of clear consecutive observations from six to four could also help COLD reduce the time lag, but it would cause an accuracy decrease larger than 10% in the F1 score (Fig. 13).

4.4. Accuracy assessment and algorithm comparisons

The accuracy assessment of NRT-MONITOR includes two parts: one is to validate the confirmed land disturbance maps and the other is to validate the unconfirmed land disturbance (or potential land disturbance) maps with different change probabilities. The optimal thresholds were determined as 30 days for the minimum time interval and 0.99999 for the change threshold when using the harmonized Landsats 7–8 and Sentinel-2 data for NRT land disturbance monitoring starting from 2015. NRT-MONITOR achieved an F1 score of 66.7 $\pm$ 1.1%, 74.0 $\pm$ 0.9%, 76.4 $\pm$ 1.0%, 69.5 $\pm$ 0.7%, 71.3 $\pm$ 0.8% for the year of 2015, 2016, 2017, 2018, and 2019, respectively. Combining the five periods, NRT-

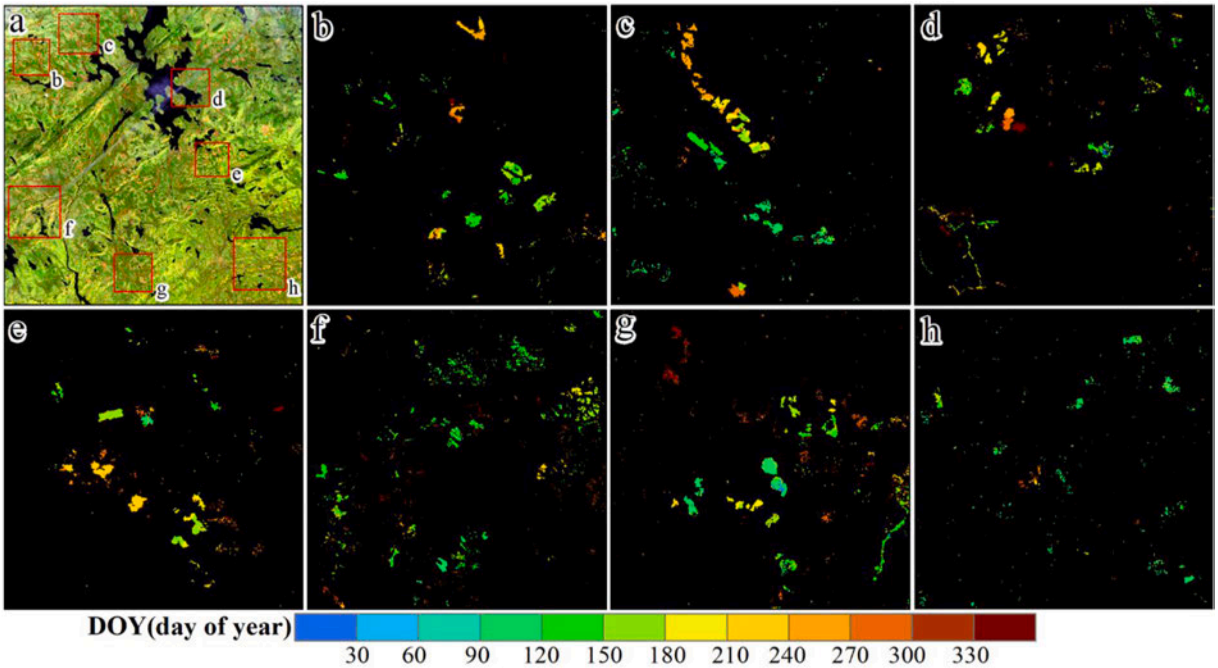

Fig. 9. Land disturbance monitoring results detected within a single year (2015, 2016, or 2017) from locations of b-h for a subset of the HLS tile T19TDL. (a) The false-color composite (R: SWIR1, G: NIR, B: R) is Landsat 8 image collected on September 26th, 2020; (b, d) The 2017 land disturbance maps for locations b and d; (c, h) The 2016 land disturbance maps for locations c and h; (e-g) The 2015 land disturbance maps for locations e, f, and g. The colors in the land disturbance maps represent the Day-Of-Year (DOY) the land disturbances were detected.

MONITOR achieved an F1 score of 69.6 $\pm$ 0.9%, with an omission error of 30.4 $\pm$ 1.0% and a commission error of 30.1 $\pm$ 1.1%. The probabilities of potential land disturbances provided by NRT-MONITOR were also evaluated. Fig. 12 shows how the commission and omission errors change when the probability of potential land disturbance changes. The commission error was high (>70%) at low probabilities of potential land disturbance, and it began to decrease when the probability reached 50%. The omission error was smaller than 15% at a low probability of potential land disturbance, and it showed an increasing trend with the increase of the probability of potential land disturbance.

We compared NRT-MONITOR with COLD in items of efficiency and accuracy. As COLD is previously not implemented in an online way, we modified COLD to be run online and compared the efficiency of NRT-MONITOR both with the original COLD (offline version) and modified COLD (online version). The 1200 HLS samples were used to compare the time efficiency of NRT-MONITOR and COLD for updating the NRT monitoring of land disturbance based on the first clear observation in 2020. The 50% of randomly selected samples were used to conduct the accuracy assessment of COLD, which followed the same evaluation procedure of NRT-MONITOR. For original COLD, as it runs on the entire time series, the running time on full historical time series ended at the first clear observation in 2020 was regarded as its time efficiency. For the modified COLD, we first saved the monitoring results and intermediate data that ended in 2019 and then updated monitoring results based on the first clear observation in 2020. It should be noted that all historical observations would still be used for current updates in the modified COLD since it requires all historical observations to re-estimate the time series model and the DOY-nearest RMSEs (Zhu et al., 2020). The monitoring results of NRT-MONITOR were updated based on the monitoring results that ended in 2019. The time efficiency of the original COLD for running 1200 samples was 869.6 s using one CPU core (Intel (R) Xeon(R) Silver 4210 CPU @ 2.20GHz), while it only took 75.9 s for NRT-MONITOR, suggesting that NRT-MONITOR was 11.5 times faster than COLD for NRT land disturbance monitoring (both implemented in MATLAB). The time efficiency of the modified COLD (MATLAB code) was 272.7 s, and it was improved by 3.2 times compared to the original COLD. While NRT-MONITOR was still 3.6 times faster than the modified COLD. Moreover, NRT-MONITOR does not need to save all historical observations, which could substantially reduce the amount of needed data storage. The accuracy of NRT-MONITOR for monitoring all land disturbances from 2015 to 2019 was very similar (0.7% difference) to that of COLD (Fig. 13). The S-CCD algorithm (C code) also improved the time efficiency by integrating Kalman Filter and it was up to 4.4 times faster than the original COLD (MATLAB code) (Ye et al., 2021), but it was designed for only monitoring forest disturbance and the accuracy for monitoring all kinds of land disturbance types was lower than that of COLD (Ye et al., 2021), especially for agricultural and urban areas.

5. Discussion and conclusion

This study developed an algorithm (NRT-MONITOR) for NRT land disturbance monitoring based on the harmonized Landsats 7–8 and Sentinel-2 data. It was developed and validated by using 1200 samples created from the harmonized Landsats 7–8 and Sentinel-2 time series from 2015 to 2019. NRT-MONITOR achieved an F1 score of 70% for monitoring all kinds of land disturbances by applying the modified TRA approach to reduce the reflectance difference between Landsats 7–8 and Sentinel-2 time series (Shang and Zhu, 2019). Without applying the modified TRA approach to conduct the reflectance adjustment, the F1 score was reduced to 49.8% (Fig. S10), indicating that the reflectance difference between Sentinel-2 and Landsat 8 and between Landsat 7 and Landsat 8 should be minimized before being used for NRT monitoring of land disturbance.

NRT-MONITOR had a mean time lag of 35 days in NRT monitoring of land disturbance, which was much faster than that of COLD ($\geq$96 days) and S-CCD ($\geq$80 days) (Ye et al., 2021; Zhu et al., 2020). This large reduction of the time lag was contributed from two aspects: first, the improved temporal frequency (from 8 to 16 days to 3 days) by harmonizing Landsats 7–8 and Sentinel-2 data contributed to reducing the time lag of NRT land disturbance monitoring; and second, the minimized time interval and minimized number of consecutive observations used in confirming a land disturbance in NRT-MONITOR also contributed to

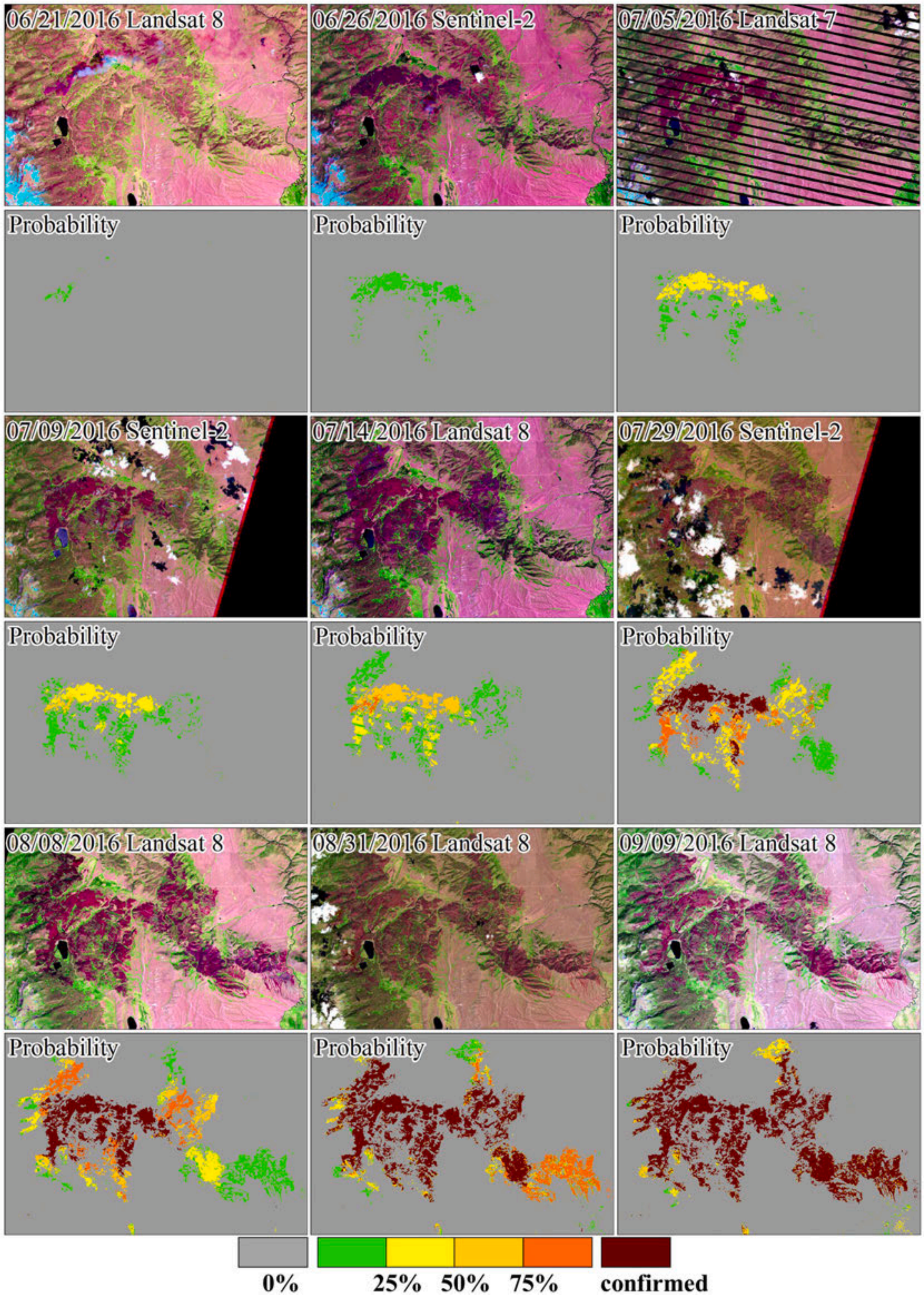

Fig. 10. An example of the land disturbance probability maps for a fire event using the harmonized Landsats 7–8 and Sentinel-2 observations. The odd rows are the false-color composites (R: SWIR1; G: NIR; B: Red). The even rows are the NRT updated land disturbance probability maps provided by NRT-MONITOR. To avoid redundancy, only several key dates are selected to show the updated probability maps of the land disturbance. (For interpretation of the references to color in this figure legend, the reader is referred to the web version of this article.)

reducing the time lag. The minimum number of clear consecutive observations was reduced from six (used both in COLD and S-CCD) to four, and the minimum time interval was reduced from 80 days in S-CCD and ~ 96 days in COLD to 30 days. For most situations, 30 days are sufficient to collect more than four clear observations, and the time lag of NRT monitoring is 30 days. But for some cloud-prone areas or wet seasons, it might be a challenge to collect four clear observations within 30 days even by harmonizing Landsats 7–8 and Sentinel-2 data, resulting in a time lag larger than 30 days. This explained why NRT-MONITOR had a mean time lag of 35 days in NRT monitoring of land disturbance. It is worth noting that reducing the number of clear consecutive observations or the time interval could cause a decrease in the monitoring accuracy,

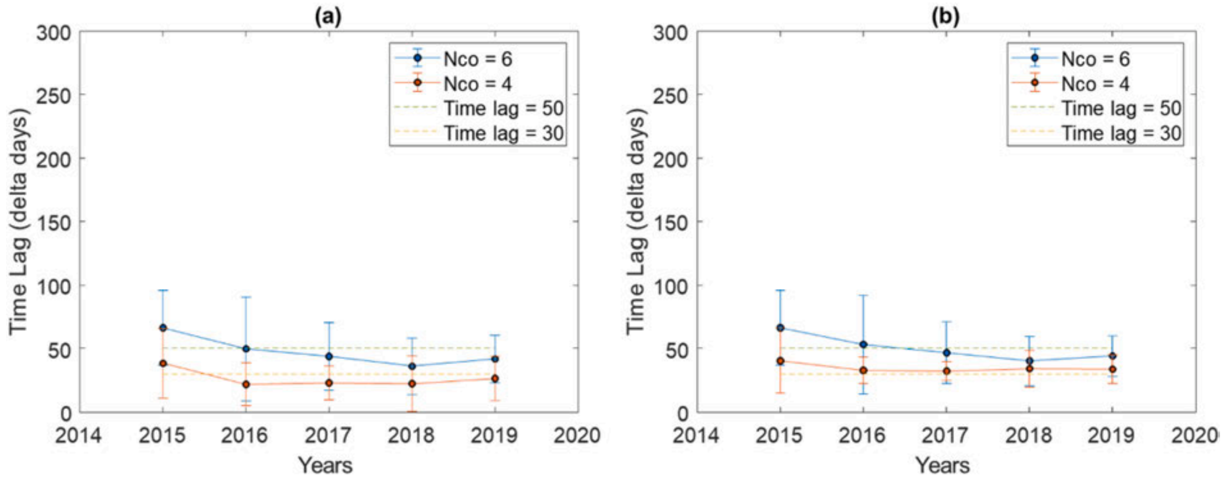

Fig. 11. The mean time lags of confirming land disturbances at each year for the 1200 HLS reference samples. (a) Without using a minimum time interval in the confirmation of land disturbance; (b) Using a minimum time interval of 30 days. "Nco" means the number of clear consecutive observations used for confirming a land disturbance.

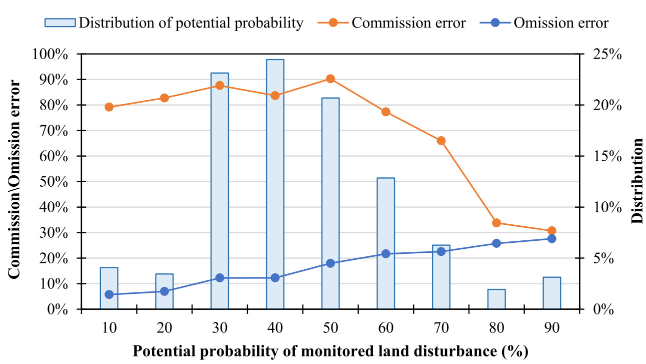

Fig. 12. The histograms of the potential probability of the monitored land disturbance and their corresponding commission and omission errors based on harmonized Landsats 7–8 and Sentinel-2 time series.

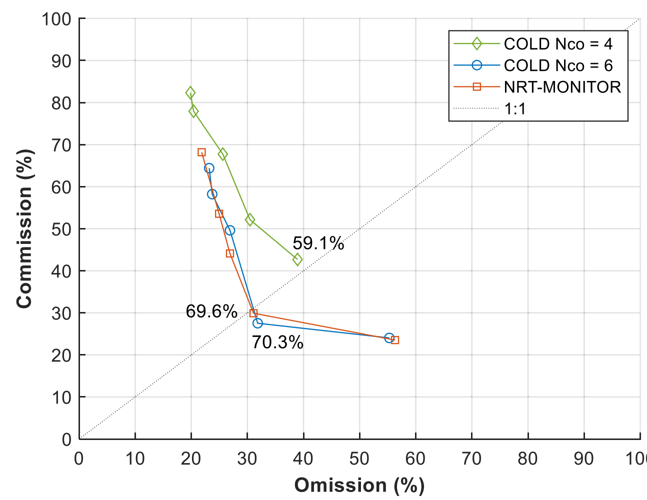

Fig. 13. Accuracy comparisons between COLD and NRT-MONITOR with different change thresholds. Nco means the number of consecutive observations used to confirm a land disturbance. Five points in the green and blue curves represent change thresholds of 0.9, 0.95, 0.99, 0.999, and 0.9999 used in COLD. Five points in the red curve represent change thresholds of 0.999, 0.9999, 0.99995, 0.99999, and 0.999999 used in NRT-MONITOR. (For interpretation of the references to color in this figure legend, the reader is referred to the web version of this article.)

but due to different algorithm designs in removing the outliers and stabilizing the recursive estimations of surface reflectance, NRT-MONITOR can reduce these two minimum thresholds to a certain degree without sacrificing the accuracy of NRT land disturbance monitoring. NRT-MONITOR was 11.5 times faster than COLD for NRT land disturbance monitoring. The time efficiency of NRT-MONITOR was mainly improved by integrating Forgetting Factor, which does not require storing all historical data and can update the land disturbance monitoring based on previous monitoring results. This is different from COLD that requires storing all historical data and re-estimate the time series model with all historical data for every new observation (Zhu et al., 2020). COLD can be implemented in an online way for NRT monitoring, and the modified COLD improved the time efficiency by 3.2 times compared to the original COLD. However, even the modified COLD is still 3.6 times slower than NRT-MONITOR.

NRT-MONITOR also had some limitations. First, the optimal thresholds determined based on the reference plots might not be optimal for every specific region or specific land disturbance agent. Local calibration of the algorithm parameters for some specific regions, land cover, or disturbance agents is recommended for future modifications. Second, the accuracy of NRT monitoring was slightly lower than that of retrospective land disturbance detection. One major reason is that the DOY-nearest RMSE, which performs well in describing seasonal changes of RMSE (Ye et al., 2021; Zhu et al., 2020), cannot be directly used for NRT monitoring of land disturbance that cannot save all historical observations. Third, harmonizing Landsat 7–8 and Sentinel-2 data at 30-m spatial resolution increased the temporal frequency, but sacrificed the higher spatial resolution (e.g., 10-m and 20-m) of Sentinel-2 data. Some data fusion methods (Shao et al., 2019; Wang et al., 2017) could be helpful to downscale 30-m Landsat observations and 20-m Sentinel-2 observations into 10-m, which has the potential to simultaneously improve the temporal and spatial resolutions for disturbance monitoring. Fourth, we did not consider the delay between the occurrence of the disturbance event and when the change in the spectral signal become large enough to be detectable in the satellite images (referred to as detectable delay), and we were only focused on reducing the time lag, which was defined as the delta days required for confirming a land disturbance after its first occurrence observed in satellite data. These two delays are different, but there is no way to quantify "detectable delay" if the signal is not large enough to be observed in the remote sensing images, unless field visits are carried out at the same time as the first occurrence of land disturbances. Last, some land disturbance events with a subtle spectral change signal might not be well captured. This is a common limitation for land disturbance monitoring algorithms. Incorporating the red-edge signals (Abdullah et al., 2019) or some new spatial-temporal approaches (Liu and Cai, 2012) is recommended to capture these land disturbance events in future modifications. The source code of NRT-MONITOR is provided in GitHub (https://github.com/GERSL/NRT-MONITOR) as a toolkit for people who need NRT land monitoring capabilities.

In conclusion, NRT-MONITOR was developed for NRT land disturbance monitoring over the CONUS based on the harmonized Landsats 7–8 and Sentinel-2 data. It achieved an overall accuracy of 70% for monitoring a variety of land disturbances. Compared to other current approaches, NRT-MONITOR had faster confirmation of land disturbance, more efficient processing time, and similar accuracy for monitoring land disturbance. Lastly, NRT-MONITOR can directly update the monitoring of land disturbance with every new observation based on previous monitoring results and provide potential land disturbance alerts every three days.

Credit authorship contribution statement

Rong Shang: Conceptualization, Methodology, Formal analysis, Validation, Visualization, Writing - original draft. Zhe Zhu: Supervision. Junxue Zhang: Formal analysis. Shi Qiu: Formal analysis. Zhiqiang Yang: Resource, Software, Writing - review & editing. Tian Li: Resource, Validation. Xiucheng Yang: Resource, Validation.

Declaration of Competing Interest

The authors declare that they have no known competing financial interests or personal relationships that could have appeared to influence the work reported in this paper.

Acknowledgments

This research was supported by the USGS-NASA Landsat Science Team Program for Toward Near Real-time Monitoring and Characterization of Land Surface Change for the Conterminous US (140G0119C0008). The authors would like to acknowledge the HLS data downloaded from https://hls.gsfc.nasa.gov/data/, and Landsat 7 Collection 1 data from Google Earth Engine. The content of this document does not necessarily represent the views or policies of the Department of the Interior, nor does mention of trade names, commercial products, or organizations imply endorsement by the U.S. Government.

Appendix A. Supplementary data

Supplementary data to this article can be found online at https://doi.org/10.1016/j.rse.2022.113073.

References

Abdullah, H., Skidmore, A.K., Darvishzadeh, R., Heurich, M., 2019. Timing of red-edge and shortwave infrared reflectance critical for early stress detection induced by bark beetle (Ips typographus, L.) attack. Int. J. Appl. Earth Obs. Geoinf. 82, 101900.
Brooks, E.B., Wynne, R.H., Thomas, V.A., Blinn, C.E., Coulston, J.W., 2014. On-the-fly massively multitemporal change detection using statistical quality control charts and landsat data. IEEE Trans. Geosci. Remote Sens. 52, 3316–3332.
Brown, J.F., Tollerud, H.J., Barber, C.P., Zhou, Q., Dwyer, J.L., Vogelmann, J.E., Loveland, T.R., Woodcock, C.E., Stehman, S.V., Zhu, Z., Pengra, B.W., Smith, K., Horton, J.A., Xian, G., Auch, R.F., Sohl, T.L., Sayler, K.L., Gallant, A.L., Zelenak, D., Reker, R.R., Rover, J., 2019. Lessons learned implementing an operational continuous United States national land change monitoring capability: the Land Change Monitoring, Assessment, and Projection (LCMAP) approach. Remote Sens. Environ. 238, 111356.
Carlson, N.A., 1973. Fast triangular formulation of the square root filter. AIAA J. 11, 1259–1265.
Chen, N., Tsendbazar, N.-E., Hamunyela, E., Verbesselt, J., Herold, M., 2021. Sub-annual tropical forest disturbance monitoring using harmonized Landsat and Sentinel-2 data. Int. J. Appl. Earth Obs. Geoinf. 102, 102386.
Claverie, M., Ju, J., Masek, J.G., Dungan, J.L., Vermote, E.F., Roger, J.C., Skakun, S.V., Justice, C., 2018. The harmonized Landsat and Sentinel-2 surface reflectance data set. Remote Sens. Environ. 219, 145–161.
Cohen, W.B., Yang, Z., Kennedy, R., 2010. Detecting trends in forest disturbance and recovery using yearly Landsat time series: 2. TimeSync - Tools for calibration and validation. Remote Sens. Environ. 114, 2911–2924.
Ding, C., Zhang, L., Liao, M., Feng, G., Dong, J., Ao, M., Yu, Y., 2020. Quantifying the spatio-temporal patterns of dune migration near Minqin Oasis in northwestern China with time series of Landsat-8 and Sentinel-2 observations. Remote Sens. Environ. 236, 111498.
Emanuel, K., 2005. Increasing destructiveness of tropical cyclones over the past 30 years. Nature 436, 686–688.
Gorelick, N., Hancher, M., Dixon, M., Ilyushchenko, S., Thau, D., Moore, R., 2017. Google Earth Engine: planetary-scale geospatial analysis for everyone. Remote Sens. Environ. 202, 18–27.
Hammer, D., Kraft, R., Wheeler, D., 2014. Alerts of forest disturbance from MODIS imagery. Int. J. Appl. Earth Obs. Geoinf. 33, 1–9.
Hamunyela, E., Verbesselt, J., Herold, M., 2016. Using spatial context to improve early detection of deforestation from Landsat time series. Remote Sens. Environ. 172, 126–138.
Hansen, M.C., Loveland, T.R., 2012. A review of large area monitoring of land cover change using Landsat data. Remote Sens. Environ. 122, 66–74.
Hansen, M.C., Potapov, P.V., Moore, R., Hancher, M., Turubanova, S.A., Tyukavina, A., Thau, D., Stehman, S.V., Goetz, S.J., Loveland, T.R., Kommareddy, A., Egorov, A., Chini, L., Justice, C.O., Townshend, J.R.G., 2013. High-resolution global maps of 21st-century forest cover change. Science 342, 850–853.
Hansen, M.C., Krylov, A., Tyukavina, A., Potapov, P.V., Turubanova, S., Zutta, B., Ifo, S., Margono, B., Stolle, F., Moore, R., 2016. Humid tropical forest disturbance alerts using Landsat data. Environ. Res. Lett. 11, 034008.
Hermosilla, T., Wulder, M.A., White, J.C., Coops, N.C., Hobart, G.W., 2015. Regional detection, characterization, and attribution of annual forest change from 1984 to 2012 using Landsat-derived time-series metrics. Remote Sens. Environ. 170, 121–132.
Homer, C., Dewitz, J., Yang, L., Jin, S., Danielson, P., Xian, G., Coulston, J., Herold, N., Wickham, J., Megown, K., 2015. Completion of the 2011 national land cover database for the conterminous United States – Representing a decade of land cover change information. Photogramm. Eng. Remote. Sens. 81, 345–354.
Huang, C., Goward, S.N., Masek, J.G., Thomas, N., Zhu, Z., Vogelmann, J.E., 2010. An automated approach for reconstructing recent forest disturbance history using dense Landsat time series stacks. Remote Sens. Environ. 114, 183–198.
Kato, A., Thau, D., Hudak, A.T., Meigs, G.W., Moskal, L.M., 2020. Quantifying fire trends in boreal forests with Landsat time series and self-organized criticality. Remote Sens. Environ. 237, 111525.
Kennedy, R.E., Yang, Z., Cohen, W.B., 2010. Detecting trends in forest disturbance and recovery using yearly Landsat time series: 1. LandTrendr - Temporal segmentation algorithms. Remote Sens. Environ. 114, 2897–2910.
Khalil, W., Dombre, E., 2004. System Identification: Theory for the User. PTR Prentice Hall, Up. Saddle River, NJ, pp. 1–14.
Liu, D., Cai, S., 2012. A spatial-temporal modeling approach to reconstructing land-cover change trajectories from multi-temporal satellite imagery. Ann. Assoc. Am. Geogr. 102, 1329–1347.
Ma, T., Zhou, Y., Zhou, C., Haynie, S., Pei, T., Xu, T., 2015. Night-time light derived estimation of spatio-temporal characteristics of urbanization dynamics using DMSP/OLS satellite data. Remote Sens. Environ. 158, 453–464.
Potapov, P., Tyukavina, A., Turubanova, S., Talero, Y., Hernandez-Serna, A., Hansen, M. C., Saah, D., Tenneson, K., Poortinga, A., Aekakkararungroj, A., Chishtie, F., Towashiraporn, P., Bhandari, B., Aung, K.S., Nguyen, Q.H., 2019. Annual continuous fields of woody vegetation structure in the Lower Mekong region from 2000-2017 Landsat time-series. Remote Sens. Environ. 232, 111278.
Qiu, S., Lin, Y., Shang, R., Zhang, J., Ma, L., Zhu, Z., 2019. Making Landsat time series consistent: evaluating and improving Landsat analysis ready data. Remote Sens. 11, 51.
Reymondin, L., Perez-Uribe, A., Argote, K., 2012. Terra-i A Methodology for Near Real-Time Monitoring of Habitat Change at Continental Scales using MODIS-NDVI and TRMM.
Roy, D.P., Zhang, H.K., Ju, J., Gomez-Dans, J.L., Lewis, P.E., Schaaf, C.B., Sun, Q., Li, J., Huang, H., Kovalskyy, V., 2016. A general method to normalize Landsat reflectance data to nadir BRDF adjusted reflectance. Remote Sens. Environ. 176, 255–271.
Roy, D.P., Huang, H., Boschetti, L., Giglio, L., Yan, L., Zhang, H.H., Li, Z., 2019. Landsat-8 and Sentinel-2 burned area mapping - a combined sensor multi-temporal change detection approach. Remote Sens. Environ. 231, 111254.
Senf, C., Seidl, R., Hostert, P., 2017. Remote sensing of forest insect disturbances: current state and future directions. Int. J. Appl. Earth Obs. Geoinf. 60, 49–60.
Shang, R., Zhu, Z., 2019. Harmonizing Landsat 8 and Sentinel-2: a time-series-based reflectance adjustment approach. Remote Sens. Environ. 235, 111439.
Shao, Z., Cai, J., Fu, P., Hu, L., Liu, T., 2019. Deep learning-based fusion of Landsat-8 and Sentinel-2 images for a harmonized surface reflectance product. Remote Sens. Environ. 235, 111425.
Tang, X., Bullock, E.L., Olofsson, P., Estel, S., Woodcock, C.E., 2019. Near real-time monitoring of tropical forest disturbance: new algorithms and assessment framework. Remote Sens. Environ. 224, 202–218.
Verbesselt, J., Zeileis, A., Herold, M., 2012. Near real-time disturbance detection using satellite image time series. Remote Sens. Environ. 123, 98–108.

Wang, Q., Blackburn, G.A., Onojeghuo, A.O., Dash, J., Zhou, L., Zhang, Y., Atkinson, P. M., 2017. Fusion of Landsat 8 OLI and Sentinel-2 MSI Data. IEEE Trans. Geosci. Remote Sens. 55, 3885–3899.

Wang, J., Xiao, X., Liu, L., Wu, X., Qin, Y., Steiner, J.L., Dong, J., 2020. Mapping sugarcane plantation dynamics in Guangxi, China, by time series Sentinel-1, Sentinel-2 and Landsat images. Remote Sens. Environ. 247.

Westerling, A.L., Hidalgo, H.G., Cayan, D.R., Swetnam, T.W., 2006. Warming and earlier spring increase Western U.S. Forest wildfire activity. Science 313, 940–943.

Wulder, M.A., Loveland, T.R., Roy, D.P., Crawford, C.J., Masek, J.G., Woodcock, C.E., Allen, R.G., Anderson, M.C., Belward, A.S., Cohen, W.B., Dwyer, J., Erb, A., Gao, F., Griffiths, P., Helder, D., Hermosilla, T., Hipple, J.D., Hostert, P., Hughes, M.J., Huntington, J., Johnson, D.M., Kennedy, R., Kilic, A., Li, Z., Lymburner, L., McCorkel, J., Pahlevan, N., Scambos, T.A., Schaaf, C., Schott, J.R., Sheng, Y., Storey, J., Vermote, E., Vogelmann, J., White, J.C., Wynne, R.H., Zhu, Z., 2019. Current status of Landsat program, science, and applications. Remote Sens. Environ. 225, 127–147.

Xin, Q., Olofsson, P., Zhu, Z., Tan, B., Woodcock, C.E., 2013. Toward near real-time monitoring of forest disturbance by fusion of MODIS and Landsat data. Remote Sens. Environ. 135, 234–247.

Ye, S., Rogan, J., Zhu, Z., Eastman, J.R., 2021. A near-real-time approach for monitoring forest disturbance using Landsat time series: stochastic continuous change detection. Remote Sens. Environ. 252, 112167.

Zhang, J., Shang, R., Rittenhouse, C., Witharana, C., Zhu, Z., 2021. Evaluating the impacts of models, data density and irregularity on reconstructing and forecasting dense Landsat time series. Sci. Remote Sens. 4, 100023.

Zhou, Q., Rover, J., Brown, J., Worstell, B., Howard, D., Wu, Z., Gallant, A.L., Rundquist, B., Burke, M., 2019. Monitoring landscape dynamics in central U.S. grasslands with harmonized Landsat-8 and Sentinel-2 time series data. Remote Sens. 11.

Zhu, Z., Qiu, S., 2022. Remote Sensing of Land Change: A Multifaceted Perspective. https://doi.org/10.1002/essoar.10510470.1.

Zhu, Zhe, Woodcock, Curtis E., 2012. Object-based cloud and cloud shadow detection in Landsat imagery. Remote Sens. Environ. 118, 83–94.

Zhu, Z., Woodcock, C.E., 2014a. Continuous change detection and classification of land cover using all available Landsat data. Remote Sens. Environ. 144, 152–171.

Zhu, Z., Woodcock, C.E., 2014b. Automated cloud, cloud shadow, and snow detection in multitemporal Landsat data: an algorithm designed specifically for monitoring land cover change. Remote Sens. Environ. 152, 217–234.

Zhu, Z., Woodcock, C.E., Olofsson, P., 2012. Continuous monitoring of forest disturbance using all available Landsat imagery. Remote Sens. Environ. 122, 75–91.

Zhu, Z., Woodcock, C.E., Holden, C., Yang, Z., 2015. Generating synthetic Landsat images based on all available Landsat data: predicting Landsat surface reflectance at any given time. Remote Sens. Environ. 162, 67–83.

Zhu, Z., Zhang, J., Yang, Z., Aljaddani, A.H., Cohen, W.B., Qiu, S., Zhou, C., 2020. Continuous monitoring of land disturbance based on Landsat time series. Remote Sens. Environ. 238, 111116.